View metadata, citation and similar papers at core.ac.uk

brought to you by CORE

provided by Loughborough University Institutional Repository

This item was submitted to Loughborough's Institutional Repository (https://dspace.lboro.ac.uk/) by the author and is made available under the following Creative Commons Licence conditions.

creative commons

COMMONS DEED

Attribution-NonCommercial-NoDerivs 2.5

You are free:

- to copy, distribute, display, and perform the work

Under the following conditions:

Attribution. You must attribute the work in the manner specified by the author or licensor.

Noncommercial. You may not use this work for commercial purposes.

No Derivative Works. You may not alter, transform, or build upon this work.

- For any reuse or distribution, you must make clear to others the license terms of this work.
- Any of these conditions can be waived if you get permission from the copyright holder.

Your fair use and other rights are in no way affected by the above.

This is a human-readable summary of the Legal Code (the full license).

Disclaimer

For the full text of this licence, please go to:
http://creativecommons.org/licenses/by-nc-nd/2.5/

Stacking faults in ultra-thin films of silver on Al(111) investigated by medium energy ion scattering

C.J. Howe[1], M.D. Cropper[1]♦, R.M. Wardle[1], P.Bailey[2] and T.C.Q. Noakes[2]

[1]. *Department of Physics, Loughborough University, Loughborough, LE11 3TU, UK*
[2]. *STFC Daresbury Laboratory, Daresbury, Warrington, WA4 4AD, UK*

Abstract

Medium energy ion scattering has been used to investigate depositions of 0.2, 1.4, 3.5 and 4.8 ML of silver onto Al(111). Energy profiles indicate alloying to the extent that aluminium is still visible after the deposition of 4.8 ML. From assessments of the visibility, blocking dips and fits using VEGAS simulations it is shown that the first two layers continue the fcc stacking but after that hcp and fcc twin-type stacking faults occur. The 1.4 ML structure is consistent with a mixed structure of 85% fcc and 15% hcp indicating that some silver occupies a third layer. The blocking curve from the structure formed by 3.5 ML equivalent deposition can be simulated by 56% fcc, 32% hcp and 12% fcc twin and that from 4.8 ML by 59% fcc, 23% hcp and 18% fcc twin. This provides direct evidence of the incidence of hcp stacking when silver is deposited onto Al(111) in the range between 2 and 5 ML.

Keywords: Medium Energy Ion Scattering; Aluminium; Silver; Surface Alloy; Ultra-thin Film; Hexagonal Close Packing.

♦ Corresponding author, m.d.cropper@lboro.ac.uk, +44 1509 223308, Fax: +44 1509 223986

1 Introduction

The study of the initial stages of growth of metal films on single-crystal metal substrates is a key theme in surface and nano- science. The behaviour of these systems is influenced by many parameters including surface and interface energies, lattice mismatch and the miscibility of the metals at the growth temperature. Possible complications in the formation of an epitaxial film include stacking faults and surface alloying. One system that at first sight may be expected to exhibit good epitaxy is silver on aluminium. The elements have similar lattice parameters (~0.9% mismatch) and in the bulk they are immiscible at room temperature, though they alloy at higher temperatures. Here we report a study of the growth of silver on Al(111) using medium energy ion scattering (MEIS).

There have been a small number of previous investigations of the system. A study of the initial growth of silver films on Al(111) by Losch and Niehus [1] utilised low energy ion scattering. For depositions up to 2 ML, the authors concluded that the films grew in a three-dimensional manner from the start, forming islands of silver, and they found no evidence of stacking faults concluding that the structure was an fcc continuation.

A very thorough study of the growth of silver films on Al(111) to 9 ML has been carried out by Kim et al [2] using low energy electron diffraction (LEED), Auger electron spectroscopy (AES), X-ray photoelectron spectroscopy (XPS),

oxygen titration and modified embedded atom method (MEAM) calculations. They presented evidence of the formation of a hcp Ag_2Al alloy at the interface and discussed the likely existence of hcp stacking within the film. Bulk Ag_2Al can be a chemically ordered intermetallic compound with two silver atoms and one aluminium atom within the unit cell of the hcp basal plane [3, 4]. Using LEED it was found that the three-fold 1×1 pattern of the substrate rapidly disappeared with deposition of silver and was gone by 1-2 ML indicating loss of long-range order (LRO), or certainly loss of order on the length scale probed by LEED. With continuing deposition, the diffracted orders started to return at 4 ML and reappeared as a six-fold 1×1 pattern. A LEED intensity analysis of a 9 ML film found that the structure was a twinned fcc structure containing similar amounts of two fcc domains rotated by 180° relative to each other. However, it was not possible to use LEED quantitatively to determine the structure of the films in the 2-4 ML region.

To investigate the 2-4 ML region, Kim et al used electron spectroscopy and oxygen titration. AES measurements of films in the region 1-2 ML showed a peak at 61 eV which has previously been ascribed to an Ag-Al Auger cross-transition, indicating alloying, for Al deposition on Ag(111) and Ag(110) [5]. The formation of an alloy was confirmed by XPS measurements showing a shift to higher binding energy of the Ag $3d_{5/2}$ similar to that seen in bulk Ag_2Al [6]. Oxygen titration measurements of the surface aluminium content, showed that alloy formation was restricted to the first 2-3 ML. Oxygen uptake by the surface fell away as the deposition increased, silver being much less reactive to oxygen than aluminium.

Based on these measurements and MEAM calculations of Ag_2Al alloy formations in the films, Kim et al proposed a model for the growth of the of silver on Al(111) to explain the loss of LRO at 2 ML followed by its recovery. They proposed that during the initial stages of film formation domains of two different structures: fcc silver that was a simple continuation of the substrate and an hcp alloy layer that registered onto the substrate in the hcp site – that is the alternative three-fold hollow that would not be occupied by the fcc continuation structure. The reasoning behind this was that Ag_2Al is hcp and it had previously been shown that silver would grow in an hcp structure for several layers on the hexagonally close packed plane of Ag_2Al [7]. These two mixed domains would account for the loss of LRO in the LEED pattern. Following several layers, the growth of pure fcc silver would occur and the LEED pattern recovers.

A subsequent investigation of the system by Fournée et al [8] utilised STM, a structural technique that does not require long range order. This study focused on imaging the dislocations that formed as a strain relieving mechanism in the growing film and substrate. For 0.2 ML deposition, silver islands of height 0.22 nm were observed. With further deposition to 0.5 ML and 1 ML a lattice of lines was observed in the substrate surface and on film islands. These were identified as Shockley partial dislocations, thought to be a strain relieving mechanism to accommodate incorporation of silver into the aluminium surface. In this model, the top layer of the surface has domains that are alternatingly registered into the “fcc” three-fold hollow (above another hollow in the second layer subsurface) and the “hcp” threefold hollow (atop

and atom in the second layer subsurface). At the domain wall this would involve a displacement of half a lattice spacing that could take up some of the strain caused by the slightly larger silver atoms. Rather than invoking an ordered intermetallic Ag_2Al, the authors of this work thought that a disordered alloy of silver and aluminium was most likely, with silver atoms being incorporated into the surface layer. The growth of the silver in this regime was not layer-by-layer, but further deposition to 5 ML produced a smooth film with most of the strain relieved. The authors of this work identified the mechanism for the loss of LRO as these stacking fault regions bounded by partial dislocations.

MEIS is a surface sensitive version of Rutherford backscattering that has previously been shown to be useful in the investigation of metal-on-metal epitaxy and surface alloying [9, 10, 11, 12, 13]. It may be used to investigate surface structure via a shadowing and blocking approach. MEIS is clearly not a reciprocal space method that requires LRO, but neither is it a local probe sensitive only to local structure. The lateral scale that it probes is somewhere between the two extremes and as such it is an ideal technique to apply to the structure of silver deposited onto Al(111) in the thickness regime where LEED is less appropriate. The aim of the work presented here was to employ MEIS to find direct evidence of hcp stacking in silver films grown on Al(111) and, if found, to determine when the stacking faults begin to appear.

In this report, we present the results of a MEIS investigation of depositions of 0.2, 1.4, 3.5 and 4.8 ML of silver onto Al(111). The measurement of energy profiles indicates that there is extensive alloying throughout the deposited material. From assessments of the visibility, blocking dips and fits using VEGAS simulations, we show that the first two layers of this alloy continue the fcc stacking but after that hcp and fcc twin-type stacking faults occur. We show what we believe to be the first direct evidence of hcp stacking in the films produced by deposition of between 2 and 5 ML of silver on Al(111).

2 Experimental

The UK National MEIS facility [14] comprises three main parts; an ion source and beamline, a scattering chamber where the MEIS experiments take place, and a surface science preparation chamber where the sample cleaning and deposition take place. All three sections are at ultra-high vacuum, with direct sample transfer between them. The scattering chamber is equipped with a goniometer that has three rotational and three translational axes, and a toroidal electrostatic ion analyser that disperses the scattered ions in energy whilst retaining their angular distribution. The preparation chamber is equipped with a sample stage with heating, low energy ion gun for crystal cleaning, a concentric hemispheres analyser for AES and a LEED optic.

During the experiment, the base pressure of the preparation chamber was 2×10^{-10} mbar. The Al(111) crystal was cleaned by cycles of sputtering using

1.8 to 0.8 keV Ar^+ ions followed by annealing to 673 K. After several cleaning cycles a clean and ordered surface was produced as determined by AES and observation of the LEED pattern. Silver was deposited onto the clean surface at 308 K using a water-cooled miniature effusion cell (manufactured by WA Technology Ltd), which was heated to 1208 K to give a deposition rate of approximately 0.1 ML per minute. The silver dose of each deposition was quantified using MEIS in a non-aligned "pseudo-random" direction. In each subsequent cleaning cycle, AES was used to ensure that all traces of silver had been removed before the crystal was annealed. A short experiment observing the LEED pattern at 55 eV with increasing deposition in the range 0 to 5 ML showed a large decrease in elastic intensity with a small recovery beyond 3 ML and a simultaneous increase in diffuse intensity. However, at this beam energy the diffracted orders were never quite extinguished.

The MEIS measurements utilised H^+ ions of 100 keV energy incident in two different alignment geometries; $[\bar{1}10]$ which is a nominal one-layer illumination, and $[\bar{2}33]$ which is a nominal two-layer alignment. As is usual with this apparatus, the data was collected in the form of two dimensional tiles that display counts versus scattering angle and ion energy. The large mass separation of the two elements involved meant that the blocking curves originating in scattering from the silver could be separated easily. The aluminium blocking curves however, were more problematic due to the low number of counts scattered by this low-Z element. Extraction was possible for the clean surface and thinner silver depositions but for the thicker silver films

the aluminium surface peak data is not presented. The scattering angles for the surface-peak blocking-curves were accurately calibrated by projecting the ion counts originating from the deep bulk of the aluminium crystal and comparing with simulations.

The blocking curves were simulated using the VEGAS routine developed at the FOM [15] with the addition of visual interface software developed at Warwick University [16]. The data were corrected for the Rutherford scattering cross-section and then calibrated into units of visible monolayers. This calibration was made by comparing simulations from the VEGAS routine with scattering data extracted from the clean aluminium surface to determine the instrumental sensitivity. The VEGAS model for the clean surface was constructed using the parameters determined in a previously published MEIS investigation [17]. A small count-conserving adjustment was applied to the data to correct for the known variation of sensitivity of the position sensitive detector across the angular range. Where data has been fitted some scaling of the simulations has been used as is common with this instrument [18], but where simulations have been simply compared with the data they have not been scaled.

The main aim of this work is to determine the stacking sequences within the structure formed by deposition of silver, both by identifying blocking dips related to each structure and by comparing the visibility of the data with that

from simulations. In the following discussions it is important to realise that the visibility of the film to MEIS will differ according to the precise stacking sequence present. Figure 1(a) is a schematic diagram of the layer-wise visibility within a five layer film of the two incident alignments that were used. In the [111] direction of an fcc crystal the layers are often labelled …ABCABC, etc. If the surface terminates on a C layer then when using the [$\overline{1}\overline{1}$0] alignment this layer shadows all successive layers giving one-layer illumination. For the [$\overline{2}\overline{3}$3] alignment ions are incident on the layers C and B, but all subsequent layers are shadowed giving two-layer illumination. In the remainder of the report, uppercase letters …ABC, etc. will be used to notate substrate layers and lower case letters …abc, etc. will be used to notate the layers in the overlayer formed by deposition.

In the event of a twin of an fcc structure, however, where the crystal may terminate …BAC the situation is very different; this is illustrated in Figure 1(b). The incidence angle that previously gave the [$\overline{1}\overline{1}$0] alignment becomes a three-layer [114]-type geometry. Similarly, the [$\overline{2}\overline{3}$3] alignment becomes a [$\overline{1}$ 1 14]-type geometry that would illuminate all the film and six layers in total in an extended structure.

In the case of hcp growth, the situation is more complex as there are two possible terminations, …ACA and …ABA; these are illustrated in Figures 1(c) and (d) respectively for a five-layer film. In each of these structures both

incidence angles illuminate several layers. The geometry that for fcc gives the [$\bar{1}$10] alignment would illuminate all five layers in a mixed hcp structure, though all but the top layer are illuminated only 50% when averaged across the two terminations. The [$\bar{2}$33] fully illuminates the top three layers, but the next two only 50% on average. This striking change in illumination means that these incident geometries can be particularly sensitive to deviations from perfect fcc stacking.

3 Results and Discussion

3.1 Energy Profiles

Figure 2 shows MEIS energy plots collected for the double-alignment one-layer geometry [$\bar{1}$10] in, [001] out (illustrated to the left of Figure 1(a)). Both plots show the peaks originating in scattering from the silver (just above 99 keV) and aluminium (near 94 keV). Superimposed on the data are simulations calculated using an energy simulation code. This code is described in more detail elsewhere [19] but has been modified to incorporate an asymmetric lineshape (exponentially modified Gaussian) as this has been shown to be important when fitting energy spectra [20].

In Figure 2(a) the scattering from the 0.2 ML data is shown. This data was selected to locate the energy of both peaks in a structure where the aluminium is clearly visible. The relative visibilities of the silver and aluminium peak suggest that all the silver atoms are located on or in the surface layer in

bulk-like sites and the fit that is superimposed confirms this. Figure 2(b) shows the energy profile following a 4.8 ML deposition of silver. In this profile, the visibility of the aluminium is drastically reduced by the silver overlayer. However, the energy position of the aluminium peak is similar to that found in Figure 2(a) rather than being shifted to lower energy as would be expected if the aluminium were completely buried. This indicates that aluminium atoms are present at, or very near the film surface either due to alloying bringing aluminium atoms to the surface, islanding making the substrate visible or alloying combined with stacking faults and disorder making slightly subsurface aluminium visible. The broken line shows the spectrum that would be expected for a pure, continuous silver film. However, the actual energy position of the aluminium surface peak is well represented by the fit to data shown by the solid line. This is a simulation for an alloy film of constant composition of 77% silver, 23% aluminium. The accuracy of this determination is good for the top three layers, but less accurate for lower layers. Regarding islanding, the previous STM work [8] indicates a continuous film by 5 ML, but it is possible that there are some differences in growth conditions here. Additionally, previous oxygen titration work indicates that alloying is largely restricted to the first three layers [2]. It is possible that our energy profile indicates an imperfect film with a combination of some roughness/islanding, alloying and the presence of stacking faults all increasing the near-surface visibility of the aluminium.

3.2 1.4 ML Deposition

The previous LEED analysis of the deposition of silver on Al(111) [2] indicated that the three-fold diffraction pattern was retained up to 2 ML. To investigate the structure in this regime, a deposition of 1.4 ML was analysed. This data is shown in Figure 3, which illustrates the angular blocking curves from the silver and aluminium atoms expressed as number of visible layers of each element for both of the alignment geometries.

A qualitative consideration of the silver blocking curves is quite revealing about the structure of the alloy film. The nominal one-layer [$\overline{1}10$] blocking curve, shown in Figure 3(a), reveals that some of the silver is shadowed; of the 1.4 ML, very slightly less than 1 ML is visible. This indicates that the alloy overlayer is predominantly stacked in the same direction as the fcc substrate. This effect is illustrated schematically in Figure 4 (a) which shows that when the alloy layers are stacked in the same direction as the substrate, the top layer atoms shadow the second layer in the [$\overline{1}10$] incident geometry. Using the nominal two-layer [$\overline{2}33$] geometry, shown in Figure 3(b), all of the silver is visible, indicating that it is mostly within the top two layers of the surface alloy.

This interpretation is confirmed by VEGAS simulations representing the four possible stacking sequences of 1.4 ML equivalents of silver contained within two surface alloy layers on the Al(111) substrate. Assuming, that the surface alloy is in a discrete layer above the aluminium, then if the final three layers of

the fcc substrate can be notated as …ABC then the two overlayers could be notated as ab, ac, ba and bc (Figure 4). The first two of these have fcc registry, that is the first layer occupies the three-fold fcc site on the Al(111) surface. The second two have a first layer occupation of the three-fold hcp site on the surface; that is hcp registry. There are also two possible stacking directions of the overlayer; ab and bc are stacked in the same direction as the fcc substrate while ac and ba are stacked in the reverse direction. In all four panels of Figure 3, the simulations of the two fcc registered sequences are represented by solid lines and the two hcp registered by broken lines. The two structures that are stacked in the fcc continuation direction are represented by black lines and those with the reverse stacking direction by grey lines. All these simulations have the silver equally distributed between the top two layers; a model in which silver was in one complete first layer followed by 0.4 ML in the second layer would overestimate the [$\bar{1}\bar{1}0$] silver visibility for the full range of physically acceptable non-structural parameters, confirming the previous interpretation of energy plots.

In Figure 3(a) it can be seen that the silver [$\bar{1}\bar{1}0$] blocking curve is best represented by simulations of “forward” stacking, that is in the same direction as the substrate. The figure shows simulations for the two possible stacking sequences for the (111) plane labelled ab and ac. The “reverse” stacking, ac, simulation indicated by the grey line, overestimates the visibility whereas the “forward” stacking, ab, simulation (black line) reproduces it closely. The latter

curve also show the dip at a nominal 90° that corresponds to the [001] outgoing direction and is present in the data.

From the [$\overline{2}33$] blocking curve for silver shown in Figure 3(b), it can be seen that both simulations reproduce the visibility correctly but that the reverse stacked simulation, represented by the grey line, has a deep dip at a nominal 84.24° that is not present in the data. This dip is due to a [110] type blocking event, but in a crystal rotated by 180° about the surface normal. It is possible that this dip is weakly present, indicating a small fraction of the silver participates in a stacking fault or that some islands that are fcc stacked are three layers high which would also put a dip here. Putting together all this evidence, it is clear that the majority of the silver in a 1.4 ML overlayer is stacked in the direction of the fcc continuation, and is within a bilayer.

A closer inspection of Figure 3(a) reveals that the silver [$\overline{1}10$] blocking curve has a weak dip near 98°. This may be due to a small fraction of silver atoms being in three-layer islands and for there to be an hcp stacking fault on this last, outermost layer. This small effect is discussed in more detail later in the report.

To determine the film site registry, it is necessary to consider the aluminium substrate blocking curves, which are shown in Figure 3(c) and (d). The key

indicator here is the visibility of the blocking curve, which is reduced compared with clean Al(111) (~3.2 for the [$\bar{1}$10] [17] and ~3.75 for the [$\bar{2}$33]). Aluminium has large thermal vibrations and a narrow shadow cone, so shadowing is poor and visibility is high even in nominal one-layer geometries. However, when 1.4 ML of silver is deposited, the visibility is reduced. A schematic of this effect is shown in Figure 4. When in fcc registry with the substrate, the silver atoms in the fcc “a” site would shadow the surface and subsurface aluminium atoms; silver atoms in the hcp site “b” would not do this. Thus, the reduced aluminium visibility indicates that the large part of the interface between the alloy and substrate does not have a stacking fault, and the silver is in the fcc “a” site.

This interpretation is confirmed by the VEGAS simulations shown superimposed on the data. The visibility of the blocking curves for the [$\bar{1}$10] (Figure 3(c)) and the [$\bar{2}$33] (Figure 3(d)) geometries is best represented by the simulations of …ABCab (black solid line) and …ABCac (grey solid line). Both structures with hcp registry (broken lines) give too high a visibility. It would be tempting to try to put an absolute number on the fcc site occupation, but care would need to be taken due to two possible sources of error. The first of these is the difficulty in accurately determining the absolute aluminium visibility given the weak scattering of aluminium compounded by shadowing by the large-Z silver atoms. The second of these is that the visibility is dependent on thermal vibrations, which cannot be determined with sufficient precision in such complex systems. However, over the full range of possible vibration

values and allowing a ±20% accuracy in determination of the visibility, the fcc site is still overwhelmingly favoured.

Putting together both of the pieces of information about the 1.4 ML data, the majority of the silver in this structure is fcc registered and stacks in the usual fcc direction without stacking faults. To correctly reproduce the difference in visibility between the [$\overline{1}$10] and [$\overline{2}$33] geometries, the silver needs to be evenly distributed across the top two layers. In these blocking curves, fitting the visibility reveals the silver occupation of each layer starting from the outermost and cannot easily distinguish alloying from islanding. The simulations reproduced here will tend to underestimate the aluminium visibility should the alloying result in surface segregation of aluminium, but this would reinforce the conclusion. Quantitative fits to this data are discussed later in the report.

3.3 4.8 ML Deposition

To evaluate the structure created by increased deposition, silver blocking curves were extracted after deposition of 4.8 ML. This data is shown in Figure 5(a) for the [$\overline{1}$10] geometry and Figure 5(b) for the [$\overline{2}$33] geometry. Also in the Figure are the results of simulations for four different structures for comparison with the data. Given that we know from the 1.4 ML structure that the first two layers up from the interface are stacked ab, then even simulating only five layers there are eight possible stacking patterns. Alloying and roughness would give regions with more or fewer layers. However, many of

these structures would exhibit similar features in the blocking curves that originate in a few key sequences of stacking, so we have elected to use a method of data analysis that we have used successfully for a similar system [9]. This method relies on simulating a small number of structures that are archetypical of stacking patterns that may be present. In this case, and with the constraint of ab for the first two layers from the substrate, the four archetypes that we have selected are abcab (fcc stacking), abacb (faulted twin), abcbc (faulted hcp) and ababa (hcp). The VEGAS simulations for these structures are shown in Figure 5. The use of similar archetypes with more or fewer layers gave very similar results, showing the conclusions to be sensitive not to the precise detail of the structure simulated, but more to the short range stacking sequences that are present.

Qualitative information may be extracted directly from Figure 5 by comparison of the blocking curves with that of fcc abcab simulations which are shown as solid black lines. The dip at 84.24° in the abcab simulation for the [$\bar{2}\bar{3}3$] geometry (Figure 5(b)) originates in a [114] type blocking event requiring four layers before it can be present and the dip at 100.03° is due to a [112] type blocking event which requires three layers to be present. For the [$\bar{1}\bar{1}0$] blocking curve (Figure 5(a)), the simulation shows a total visibility of about 1.8 ML with a large [001] dip at 90°. The experimental data, however, shows an increased visibility indicating a deviation from continuation fcc stacking. This increase in visibility is mirrored in the [$\bar{2}\bar{3}3$] data, which is more visible than the fcc simulation by a whole monolayer. In combination, the visibilities of

these two datasets provide clear evidence that by 5 ML the deposition of silver films has resulted in deviation from normal fcc stacking.

The origin of this increase in visibility can be found by considering the simulations of the other three archetypical structures also shown in Figure 5(a) and (b). All the three structures show, as expected, an increased visibility over the fcc simulation. The visibility of the actual data lies between that of the fcc simulation and that of the others indicating that despite the presence of stacking faults, substantial amounts of fcc stacking must still be present. The simulations also contain the additional blocking dips that are to be found in the data and that “fingerprint” the structures that are present.

The simulations for the “faulted twin” structure abacb are shown as broken black lines in Figure 5. The key features of this structure are a strong dip at 84.24° in the [$\overline{1}\overline{1}$0] geometry and another at the same angle in the [$\overline{2}\overline{3}$3] geometry. The former originates from a [33$\overline{2}$] type blocking event in the twinned lattice and requires three layers of reverse stacking to be present – the minimum definition of an fcc twin. The latter results from a [110] type blocking event, but requires only two layers to be present, that is this dip is the key signature of reverse stacking but not of genuine twinning. Although the [$\overline{2}\overline{3}$3] blocking curve does show a deep dip near 84.24° that is not found with pure fcc stacking, the data has a new dip near 94.6° that is not reproduced by the twin simulation. In addition, significant twinning would produce a dip at

84.24° in the [$\bar{1}\bar{1}0$] blocking curve that is not seen in the experimental data, and does not create the dip near 98° that is seen in the data. Thus, although a reverse stacked fcc structure may be present in the 4.8 ML film, this will affect only a small proportion of the silver atoms and in particular the [$\bar{1}\bar{1}0$] experimental blocking curve rejects large amounts of twinning.

Also shown in Figure 5 as grey lines are the simulations for two different domains of hcp stacking. These both show the expected increase in visibility, and also reproduce the additional dips seen in the data. In Figure 5(a) it can be seen that both hcp domains produce the new dip near 98° in the [$\bar{1}\bar{1}0$] blocking curve, which is a dip that would appear as soon as there were three continuous layers stacked hcp (Figure 4(c) and (d)). The continuous ababa hcp structure also produces a new dip near 86° which is just apparent in the data. In Figure 5(b) it can be seen that both hcp structures would give the increase in depth of the 84.24° blocking dip for the [$\bar{2}\bar{3}3$] geometry and the new dip near 94.6°. This latter dip appears when four continuous layers of hcp stacking are present or when three layers of aca hcp occur above a “b” type layer. Thus we have direct evidence that silver participates in an hcp structure when deposited onto the Al(111) surface to form an alloy.

3.4 Quantitative Analysis

The evolution of the structure of the alloy overlayer with increasing silver deposition is shown in Figure 6. The scattering from silver following 0.2 ML

deposition is indicated using circles, that from 1.4 ML by triangles, that from 3.5 ML by squares and that from 4.8 ML by diamonds. The solid lines in the figure represent the results of a fitting procedure that will be discussed later.

The data for the nominal two-layer [$\overline{2}33$] incidence geometry, shown in Figure 6(b), has all of the silver visible for the 0.2 ML and (previously discussed) 1.4 ML structures, which indicates that the silver is present in the top two layers of the structure. Notice however, that the visibility of the silver in the 3.5 ML structure is higher than the ~2.1 ML that is expected for a simple fcc continuation, similar to that in the 4.8 ML film. This shows clearly, that even by 3.5 ML a significant fraction of the silver is not in the fcc continuation. The dip near 94.6° which requires four layers of hcp is clearly apparent. Thus the onset of the change from perfect fcc continuation to a structure containing hcp happens between 1.4 ML and 3.5 ML total deposition. Bear in mind that film roughness may mean that some regions of the alloy film are thicker than the nominal layer coverage, while some may be thinner.

In the [1$\overline{1}$0] blocking curves the same effect can be seen. The visibility of the 3.5 ML curve is larger than the expected 1.6 ML for this one-layer alignment being around 1.9 ML. In addition, the hcp related dip near 98° is readily apparent. In the 1.4 ML curve, previously considered, a weak dip at this angle can also be observed indicating that although the 1.4 ML data is dominated by fcc stacking, there is some silver participating in the third layer below the

surface and that atoms above this are stacked hcp. This geometry confirms that by 3.5 ML the silver has departed from fcc stacking, and in fact that the beginnings of this are seen even with the start of formation of the third layer.

Fitting of the simulations of the various stacking patterns to the data can be used to extract quantitative information about the structure. As mentioned earlier, the actual structure will be a complicated mix of stacking patterns and a full simulation would require more parameters than may be accurately determined from the data. However, it is possible to determine information about the structure using a simpler approach with simulations of the archetypical structures presented in Figure 5. The line superimposed on the 1.4 ML data in Figure 6 is the result of such fitting. The basic models used here were fcc and aba hcp as although the deposition is nominally less than two layers, the dip at 98° indicates some silver is intermixed into the third layer. The result of this fit was 85% fcc and 15% hcp. One possible influence on the ion yield that should be mentioned is the effect of surface relaxation. The difference between the [111] interlayer distances for aluminium and silver is 2 pm, which is at the limit of accuracy for the technique given the number of other parameters involved. Shifts in d-spacing of this order have negligible effects on the ion yield and as there is no compelling evidence from the positions of the major dips for significant relaxation, the simulated were calculated using the bulk lattice values.

For the 4.8 ML data, a linear combination of the simulations of the four basic structures illustrated in Figure 5 was fitted simultaneously to the two blocking curves. The result of this procedure is shown superimposed on the data in Figure 6 as a solid line. This curve used represents a structure containing 23% hcp (mostly non-faulted) and 18% of the twin-like stacking sequence (uncertainty in both around 5%) The remaining 59% was the fcc continuation curve (uncertainty around 10%), though it should be noted that this fraction may contain some disordered material that gives no dips rather than the weak fcc dips. The amount of disordered material cannot be large, however, as there is a clear visibility difference between the two geometries, an effect that would not be seen with completely disordered material. This fit shows that despite the obvious departure from perfect fcc continuation stacking, the film structure still contains a large fraction that is neither hcp nor twin. Note that the dips in the simulation of the [$\overline{1}\overline{1}$0] geometry have greater depth than those in the data: this may reflect the fraction of disordered material in the alloy, giving unstructured silver visibility.

Careful inspection of Figure 6 indicates that the model underestimates the width of the dips in the [$\overline{1}\overline{1}$0] blocking curves and overestimates it in the [$\overline{2}\overline{3}$3] blocking curves. This may reflect the difference in the shadow cone width for silver and aluminium. If so it would suggest that the regions of alloy that exhibit the normal fcc stacking direction would have a larger component of silver on silver and those that exhibit hcp stacking have more aluminium on silver.

The fitting procedure for the 3.5 ML data used four different basic structures; abca (fcc), abac (faulted twin), abcb (faulted hcp) and abab (hcp). This model, which is shown in Figure 6, gave 32% hcp and 12% twin-like - a similar pattern to the thicker film, but with some more hcp. Again the remainder of the model was fcc, but may contain some disordered material. The difference between the two is on the edge of significance, but the increased depth of the 84.24° dip in the [$\overline{2}\overline{3}3$] data from the structure formed by the deposition of 4.8 ML of silver seems to indicate an increase in twinned fcc over the thinner film. The curves illustrate clearly that when MEIS is used in alignment with the fcc lattice, it is very sensitive to any deviation from this and is thus an ideal method to investigate such growth. The deviation from fcc growth is mostly of hcp type, with less of the twinning structure represented by acb type stacking.

We have shown that when silver is deposited on Al(111) then for the first two monolayer equivalents the growth is largely fcc-like ABCab, but beyond this stacking faults develop leading to both hcp-like aba and aca and twin-like acb sequences. We have shown direct evidence for the existence of hcp stacking proposed by Kim et al [2] for the thickness regime in which there is loss of LEED pattern. Their model suggested that the development of hcp like domains was due to alloying between silver and aluminium to produce hcp Ag_2Al. We have shown that in the first two layers the growth is fcc continuation with hcp developing later. Of course, when there are only two layers there is no difference between one of the hcp domains and the fcc continuation. Thus the hcp structure that is present at 3.5 layers must grow

with fcc registry for the first two layers. The visibility of the aluminium falls away rapidly with silver coverage so that the Al surface peak is difficult to observe for data extraction. However, the 32% hcp structure observed if it were due to an alloy, either chemically ordered or disordered Ag_2Al, would require a minimum of 11% Al per layer, which is well within the analysis shown in Figure 2. The growth of elemental silver in an hcp structure on Ag_2Al has been previously observed [7], so this also may contribute. The alloy overlayer contains a mix of fcc, hcp and twin, which would result in a mismatch at domain boundaries.

4 Summary

We have investigated the structures formed by the deposition of 0.2, 1.4, 3.5 and 4.8 ML films of silver upon the Al(111) surface by using MEIS. It is found that in the first two layers the silver occupies sites that continue the fcc stacking of the substrate, but after this stacking faults appear inducing both hcp and twin growth. Despite this, the faulted regions occupy around only half of the overlayer. Of the two faulted structures, there is more hcp than twin present.

5 Acknowledgements

This work was supported by the EPSRC and Loughborough University which provided studentships for CJH and RMW. Thanks are due to the FOM for the VEGAS codes and special thanks are always due to Paul Quinn for his work

on the simulations software suite. Technical assistance was provided by Mark Pendleton.

6 References

[1] A. Losch and H Niehus, Surface Science 446 (2000) 153.
[2] S. H. Kim, J. Seo, Y. Shin, W. Kim, C. Y. Park, S. –J. Oh, J. M. Seo, H. G. Min, J. –S. Kim, Physical Review B 63 (2001) 085414
[3] J. P. Neumann, Acta Metallurgica 14 (1966) 505
[4] N. A. Zarkevich, D. D. Johnson, A. V. Smirnov, Acta Materialia 50 (2002) 2443
[5] W. J. Wytenburg, R. M. Ormerod, R. M. Lambert, Surface Science 282 (1993) 205
[6] J. C. Fuggle, E. Kallne, L. M. Watson, D. J. Fabian, Physical Review B 16 (1992) 2727.
[7] E. Wetli, M. Hochstrasser, M. Erbudak, Surface Science 377-379 (1997) 876.
[8] V. Fournée, J. Ledieu, T. Cai, P. A. Thiel, Physical Review B 67 (2003) 155401
[9] M.T. Butterfield, M.D. Crapper, T.C.Q. Noakes, P. Bailey, G.J. Jackson and D.P. Woodruff, Physical Review B 62 (2000) 16984.
[10] M.D. Cropper, T.C.Q. Noakes, M.T. Butterfield, P. Bailey, Surface Science 594 (2005) 212
[11] P.C. Dastoor, D.J. O'Connor, D.A. MacLaren, W. Allison, T.C.Q. Noakes, P. Bailey, Surface Science 588 (2005)101.
[12] T. C. Q. Noakes, P. Bailey, D. T. Dekadjevi, M. A. Howson, Physical Review B 68 (2003) 097335
[13] C.J. Howe, M.D. Cropper, T.P. Fleming, R.M. Wardle, P. Bailey, T.C.Q. Noakes, Surface Science 604 (2010) 201
[14] P. Bailey, T.C.Q. Noakes, D.P.Woodruff, Surface Science 426 (1999) 358.
[15] R. M. Tromp and J. F. van der Veen, Surface Science 133 (1983) 159.
[16] XVegas Version 132, Paul Quinn, (2005).
[17] D. J. O'Connor, E. R. Wouters, A. W. Denier van der Gon, J. F. van der Veen, P. M. Zagwin, J. W. M. Frenken, Surface Sience 296 (1993) 131.
[18] P. D. Quinn, D. Brown, D. P. Woodruff, P. Bailey, T. C. Q. Noakes, Surface Science 511 (2002) 43-56.
[19] P. D. Quinn, N. R. Wilson, S. A. Hatfield, C. F. McConville, G. R. Bell, T. C. Q. Noakes, P. Bailey, S. Al-Harthi, F. Gard, Applied Physics Letters 87 (2005) 153110.
[20] P. L. Grande, A. Hentz, R. P. Pezzi, I. J. R. Baumvol, G. Schiwietz, Nuclear Instruments and Methods in Physics Research B 256 (2007) 92.

Figure 1: A schematic showing the illumination of the layers in different stacking patterns for a five layer film using both the [$\bar{1}$10] and [$\bar{2}$33] incident geometries. The [$\bar{1}$10] and [$\bar{2}$33] respectively illuminate: (a) one and two layers in fcc …ABC stacking; (b) three layers and six layers in the twin …BAC stacking; (c) odd layers and odd layers plus layer two in hcp …ACA stacking; (d) even layers plus layer one and layers one to four in hcp …ABA stacking. Some key blocking directions are indicated.

Figure 2: Energy plots for the structures formed by the deposition of (a) 0.2 ML of silver and (b) 4.8 ML of silver. The data were collected in the [$\bar{1}$10] incidence geometry with [001] take-off to give one-layer sensitivity. The solid and broken lines are the results of fits to the data as discussed in the text.

Figure 3: The silver (●) and aluminium (○) blocking curves from 1.4 ML of silver deposited on Al(111) using the [$\bar{1}$10] and [$\bar{2}$33] incidence geometries. The silver blocking curves are compared with simulations for the two possible stacking directions. The aluminium blocking curves are compared with simulations for the two possible three-fold sites for the first layer combined with the two possible stacking directions. The simulations are for 70% occupation of each of two layers by silver.

Figure 4: The effect of site and stacking faults on the illumination of specific layers in a bilayer silver film on a Al(111) terminating …ABC. (a) For the [$\bar{1}$10] incidence geometry the silver and aluminium illumination respectively is: two

and zero layers for …ABCac; one and zero layers for …ABCab; two and one layer for …ABCba; one and one layers for …ABCbc. (b) For the [$\bar{2}33$] incidence geometry the silver and aluminium illumination respectively is: two and one layers for …ABCac; two and zero layers for …ABCab; two and two layer for …ABCba; two and two layers for …ABCbc. The two key blocking directions are indicated.

Figure 5: Silver blocking curves (●) in (a) the [$\bar{1}10$] and (b) the [$\bar{2}33$] incidence geometries for the 4.8 ML overlayer. The curves are compared with the simulations for four five-layer archetypical structures registered with the first two layers registered …ABCab onto the substrate.

Figure 6: Silver blocking curves for 0.2 (○), 1.4 (∇), 3.5 (□) and 4.8 ML (◇) deposition onto Al(111) using (a) the [$\bar{1}10$] and (b) the [$\bar{2}33$] incidence geometries. Superimposed are VEGAS models that have been fitted as described in the text.

Figure 1

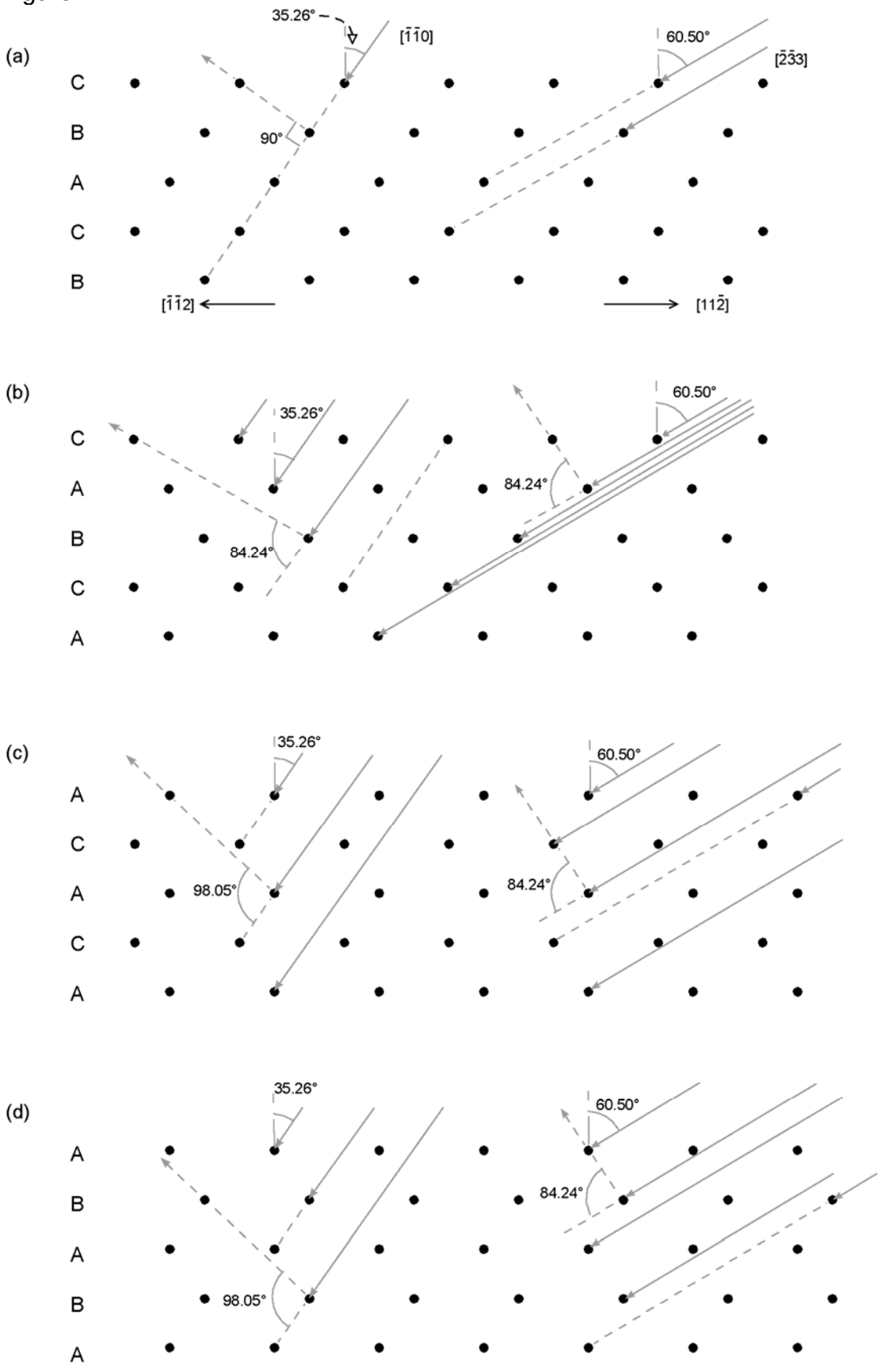
(a)
35.26°
[1̄1̄0]
60.50°
[2̄3̄3]
C
B
A
C
B
90°
[1̄1̄2]
[11̄2̄]
(b)
35.26°
60.50°
C
A
B
C
A
84.24°
84.24°
(c)
35.26°
60.50°
A
C
A
C
A
98.05°
84.24°
(d)
35.26°
60.50°
A
B
A
B
A
98.05°
84.24°

Figure 2

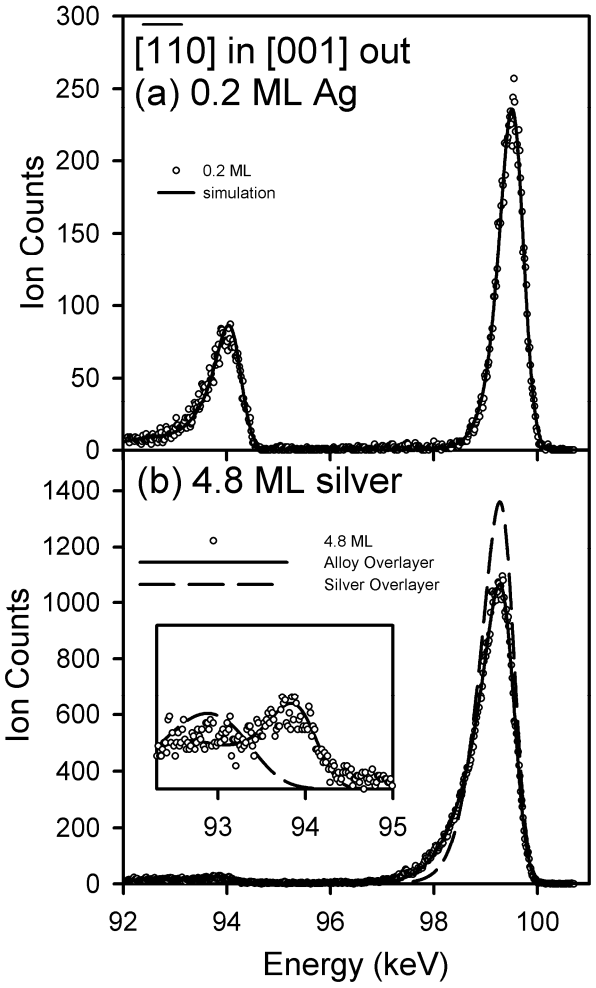
[1̄10] in [001] out
(a) 0.2 ML Ag
0.2 ML
simulation
(b) 4.8 ML silver
4.8 ML
Alloy Overlayer
Silver Overlayer
Ion Counts
Energy (keV)

Figure 3

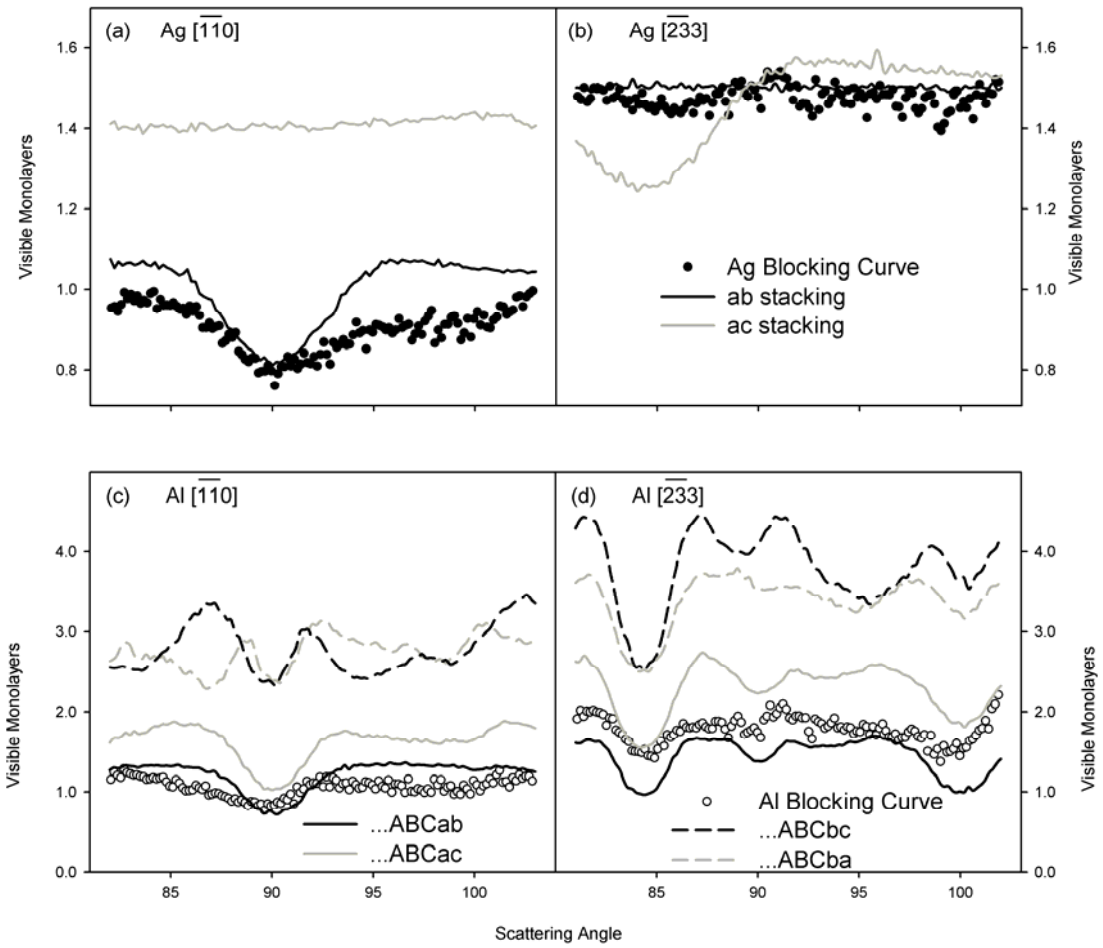
(a) Ag [$\bar{1}$10]
(b) Ag [$\bar{2}$33]
(c) Al [$\bar{1}$10]
(d) Al [$\bar{2}$33]
Visible Monolayers
Scattering Angle
Ag Blocking Curve
ab stacking
ac stacking
Al Blocking Curve
...ABCab
...ABCac
...ABCbc
...ABCba

Figure 4

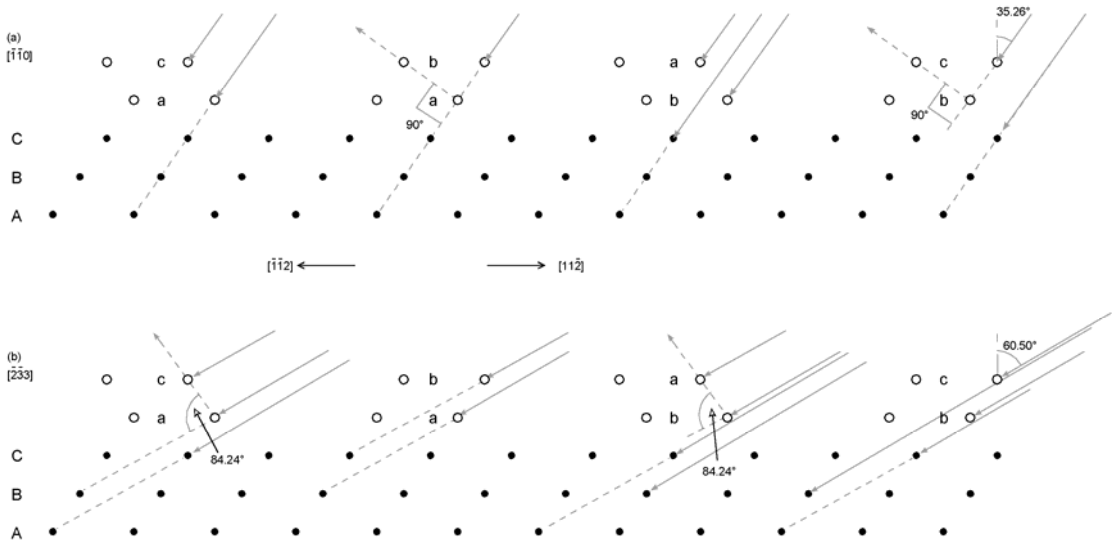
(a)
[1$\bar{1}$0]
c
a
b
a
a
b
c
b
90°
90°
35.26°
C
B
A
[$\bar{1}\bar{1}$2]
[11$\bar{2}$]
(b)
[$\bar{2}\bar{3}$3]
c
a
b
a
a
b
c
b
84.24°
84.24°
60.50°
C
B
A

Figure 5

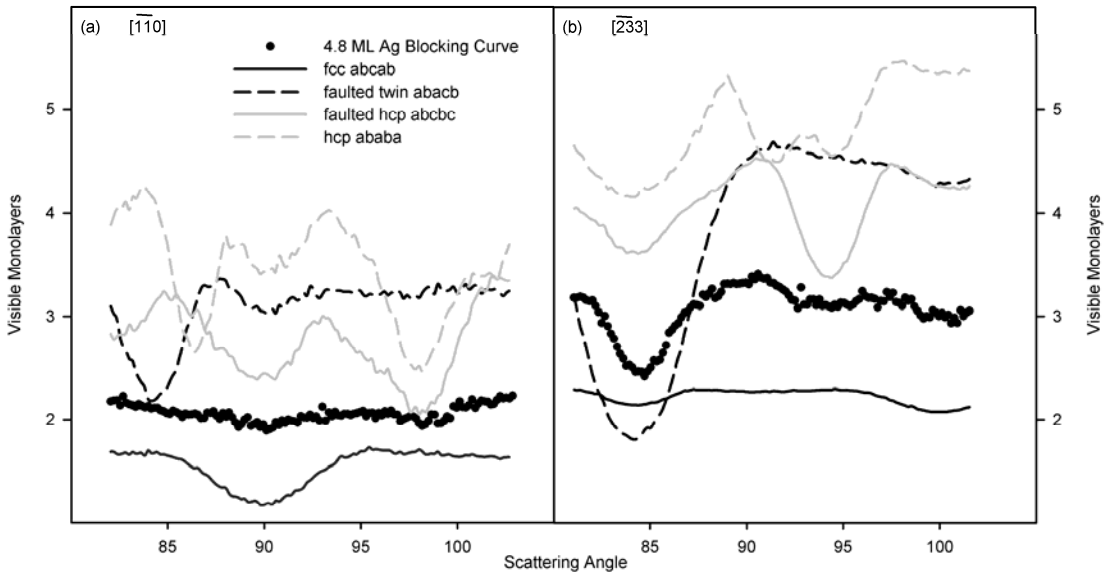
(a) [$\bar{1}10$]
(b) [$\bar{2}\bar{3}3$]
4.8 ML Ag Blocking Curve
fcc abcab
faulted twin abacb
faulted hcp abcbc
hcp ababa
Visible Monolayers
Visible Monolayers
Scattering Angle
2
3
4
5
85
90
95
100

Figure 6

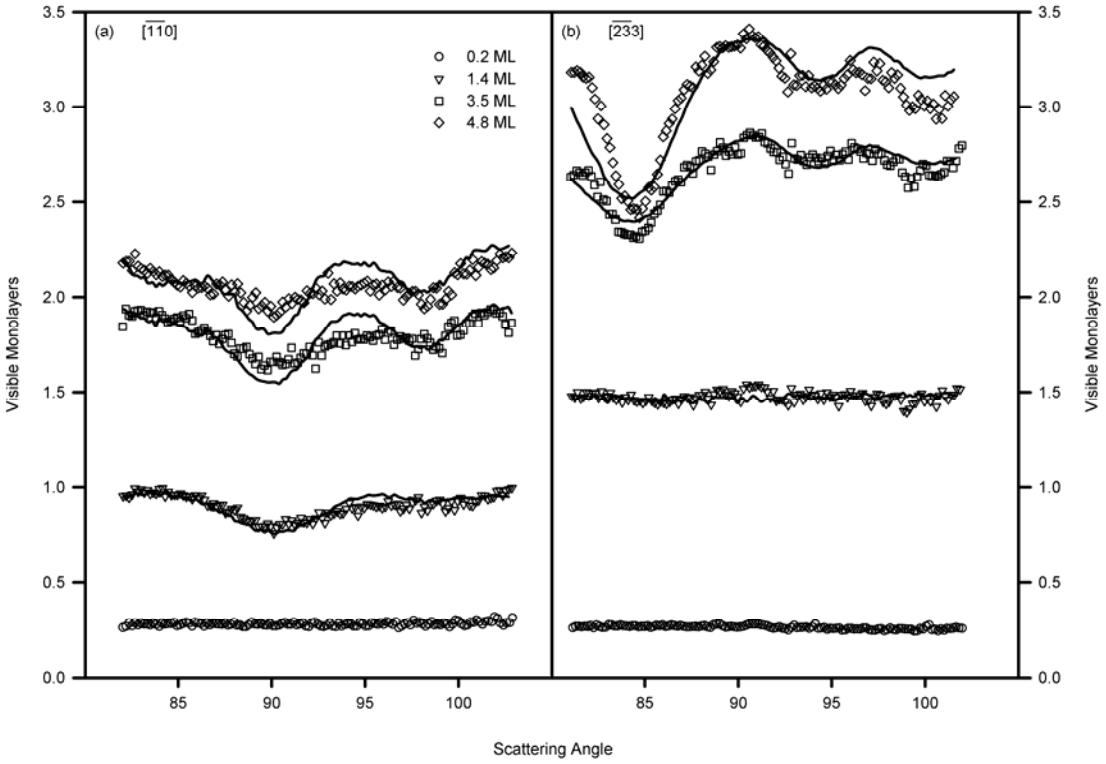
(a) [$\bar{1}\bar{1}$0]
(b) [$\bar{2}\bar{3}$3]
0.2 ML
1.4 ML
3.5 ML
4.8 ML
Visible Monolayers
Visible Monolayers
Scattering Angle
0.0
0.5
1.0
1.5
2.0
2.5
3.0
3.5
85
90
95
100